

An experimental and theoretical investigation of spray characteristics of impinging jets in impact wave regime

N. S. Rodrigues · V. Kulkarni · J. Gao · J. Chen ·
P. E. Sojka

Received: 10 October 2014 / Revised: 19 January 2015 / Accepted: 20 January 2015 / Published online: 20 February 2015
© Springer-Verlag Berlin Heidelberg 2015

Abstract The current study focuses on experimentally and theoretically improving the characterization of the drop size and drop velocity for like-on-like doublet impinging jets. The experimental measurements were made using phase Doppler anemometry (PDA) at jet Weber numbers We_j corresponding to the impact wave regime of impinging jet atomization. A more suitable dynamic range was used for PDA measurements compared to the literature, resulting in more accurate experimental measurements for drop diameters and velocities. There is some disagreement in the literature regarding the ability of linear stability analysis to accurately predict drop diameters in the impact wave regime. This work seeks to provide some clarity. It was discovered that the assumed uniform jet velocity profile was a contributing factor for deviation between diameter predictions based on models in the literature and experimental measurements. Analytical expressions that depend on parameters based on the assumed jet velocity profile are presented in this work. Predictions based on the parabolic and 1/7th power law turbulent profiles were considered and show better agreement with the experimental measurements compared to predictions based on the previous models. Experimental mean drop velocity measurements were compared with predictions from a force balance analysis, and it was observed that the assumed jet velocity profile also influences the predicted velocities, with the turbulent profile agreeing best with the experimental mean

velocity. It is concluded that the assumed jet velocity profile has a predominant effect on drop diameter and velocity predictions.

List of symbols

b^*	Dimensionless distance from center of jet to separation point (—)
d_D	Predicted drop diameter (μm)
d_j	Jet diameter (mm)
d_0	Orifice diameter (mm)
D_{10}	Arithmetic mean drop diameter (μm)
D_{32}	Sauter mean drop diameter (μm)
f_0	Number pdf (μm^{-1})
f_2	Area pdf (μm^{-1})
f_3	Volume pdf (μm^{-1})
Fr_j	Jet Froude number (—)
K^*	Dimensionless sheet thickness parameter (—)
MMD	Mass median diameter (μm)
q^*	Dimensionless radial distance from the separation point (—)
q_j^*	Dimensionless location of the jet interface (—)
R_j	Jet radius (mm)
Re_D	Drop Reynolds number (—)
Re_j	Jet Reynolds number (—)
s	Ratio of ambient gas density to liquid density (—)
U_j	Jet velocity (m s^{-1})
U_d	Drop velocity (m s^{-1})
$U_{z\text{-mean}}$	Experimentally measured mean drop velocity (m s^{-1})
We_d	Drop Weber number (—)
We_j	Jet Weber number (—)
L/d_0	Internal length-to-orifice diameter ratio (—)
x/d_0	Free jet length-to-orifice diameter ratio (—)
α	Ratio of sheet velocity to jet velocity (—)

N. S. Rodrigues (✉) · V. Kulkarni (✉) · J. Gao · J. Chen ·
P. E. Sojka

School of Mechanical Engineering, Purdue University,
West Lafayette, IN 47906, USA
e-mail: neilrodrigues@asme.org

V. Kulkarni
e-mail: vk.1421985@gmail.com

γ	Liquid/gas surface tension (N/m)
θ	Half-impingement angle ($^{\circ}$)
μ_1	Liquid viscosity (Pa s)
ρ_g	Ambient gas density (kg m^{-3})
ρ_1	Liquid density (kg m^{-3})
ϕ	Sheet azimuthal angle ($^{\circ}$)

1 Introduction

Common injectors for liquid rocket engines include the impinging jet injector (Anderson et al. 1995), coaxial injector (Vingert et al. 1995), and pintle injector (Heister 2011). Among these, the impinging jet injector is considered to be the most popular due to ease in fabrication, desirable atomization characteristics, and high-performance mixing. An impinging jet atomizer with two jets of the same liquid (either fuel or oxidizer) is called a like-on-like doublet. In contrast, an unlike doublet consists of one jet of fuel and one jet of oxidizer (Gill and Nurick 1976).

Since the injection, atomization, mixing, and combustion occur nearly simultaneously in a fuel/oxidizer system, uncoupling is required to separately investigate each of these processes (Humble et al. 1995). For instance, in liquid impinging jet atomization studies, water has been traditionally used instead of the propellant to eliminate the combustion process.

The dimensionless parameter that is typically used to characterize impinging jet atomization is the jet Weber number We_j ,

$$We_j = \frac{\rho_1 U_j^2 d_j}{\gamma}, \quad (1)$$

which represents the ratio of the inertial force to the surface tension force. In the above equation, ρ_1 is the liquid density, U_j is the jet velocity, d_j is the jet diameter (assumed to be equal to the orifice diameter d_0), and γ is the liquid–gas surface tension. Another parameter that influences the atomization process is the ratio of ambient gas density to liquid density s ,

$$s = \frac{\rho_g}{\rho_1}, \quad (2)$$

where ρ_g denotes the ambient gas density. The flow behavior of the jets (laminar or turbulent) is also of importance and is characterized by the jet Reynolds number Re_j ,

$$Re_j = \frac{\rho_1 U_j d_j}{\mu_1}, \quad (3)$$

which represents the ratio of the inertial force to the viscous force. In the above equation, μ_1 is the liquid viscosity.

Representative diameters typically used to characterize the impinging jet spray include the arithmetic mean

diameter D_{10} , Sauter mean diameter D_{32} , and the mass median diameter MMD. The arithmetic mean diameter is a first-order mean and is used widely for comparison. The Sauter mean diameter is a fifth-order mean that represents the volume-to-surface area ratio. The mass median diameter is defined as a representative diameter such that 50 % of total liquid volume is in drops of smaller diameters. The expressions to calculate these diameters are:

$$D_{10} = \frac{\sum N_i D_i}{\sum N_i}, \quad (4)$$

$$D_{32} = \frac{\sum N_i D_i^3}{\sum N_i D_i^2}, \quad (5)$$

$$0.5 = \int_0^{\text{MMD}} f_3(D) dD. \quad (6)$$

N_i and D_i are the number of drops and the drop diameters, respectively, for the mean diameter calculations. D_{32} is the most applicable mean diameter for combustion purposes because it best describes the fineness of the spray. In Eq. 6, f_3 symbolizes the volume probability density function (pdf). The volume pdf is the probability density that a drop has a volume of $\pi D^3/6$. Two other methods to quantify the polydisperse nature of the impinging jet spray are the number pdf f_0 (probability density that a drop has diameter D) and the area pdf f_2 (probability density that a drop has surface area πD^2) (Lefebvre 1989).

The atomization mechanism for the impinging jet injector with a like-on-like doublet configuration involves two cylindrical liquid jets with equal jet velocity and jet diameter impinging each other. This impingement first creates a flat liquid sheet that is perpendicular to the momentum vectors of the two jets. Instabilities are present on this liquid sheet that promote breakup. The general breakup behavior is the sheet disintegrating into ligaments and the ligaments then disintegrating into drops. Figure 1 provides a schematic of this breakup process. Disintegration is primarily caused by the aerodynamic and inertial forces and is opposed by the surface tension force. The liquid viscosity acts as a dampener for breakup—liquids possessing higher viscosity tend to break up into relatively larger drops. Since water is typically used as the test liquid for impinging jet studies, an inviscid analysis sufficiently describes the physics.

Breakup patterns in the three regimes of impinging jet atomization evolve as the jet Weber number and the jet Reynolds number increase. However, clear boundaries for breakup patterns are not reported due to the influence of injector geometry, among other factors. The following approximate conditions are summarized from Anderson et al. (2006) and von Kampen et al. (2006). The laminar

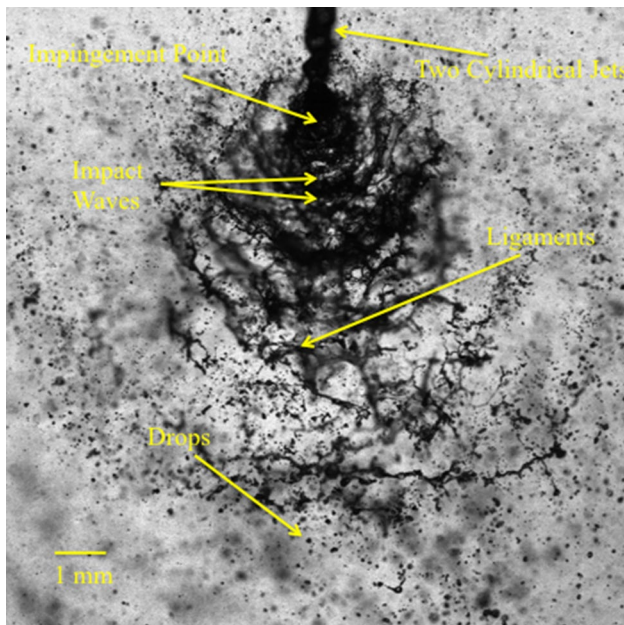


Fig. 1 Impinging jet spray formation

sheet regime is observed at lower jet Weber and jet Reynolds numbers. Patterns in this regime include the closed rim with droplet formation pattern ($We_j = 160$, $Re_j = 2480$), the open-rim pattern ($We_j = 320$, $Re_j = 3450$), and the rimless separation pattern ($We_j = 670$, $Re_j = 5020$). The impact wave regime occurs at higher jet Weber and Reynolds numbers. Patterns in this regime include the ligament structure pattern ($We_j = 3420$, $Re_j = 10,030$) and the fully developed pattern ($We_j = 19,650$, $Re_j = 23,740$). Notable features of this regime include impact waves emitting from the impingement point and a large number of small drops. The aerodynamic breakup and atomization regime are also observed but only at conditions of high ambient gas density. Only the impact wave and the aerodynamic breakup and atomization regimes occur in practical liquid rocket engines.

Previous experimental studies have investigated scaling relationships between the inertial force (often controlled using the jet velocity) and spray characteristics such as frequency of waves, sheet breakup length, drop diameter, and drop velocity. The study by Heidmann et al. (1957) was one of the earliest works that studied the frequency of waves; frequency was observed to increase with jet velocity. Anderson et al. (1992) studied the sheet breakup length; sheet breakup length is observed to decrease with an increase in the jet velocity.

Dombrowski and Hooper (1963) studied the effect of varying jet velocity on the D_{32} mean diameter for both laminar and turbulent jets. In the turbulent case, the mean drop size was observed to decrease with increasing jet velocity.

The drop size was quantified in the central region of the spray using still photography. Still photography using the shadowgraphy technique with image analysis has also been extensively applied in other impinging jet atomization studies. However, as a two-dimensional measurement technique, it only resolves characteristics in/near the focal plane of the imaging lens. Furthermore, small drops are typically not measured due to the limited dynamic range. Images are usually analyzed in the plane of the sheet formed by the two jets.

The most widely referenced literature of impinging jet atomization with phase Doppler anemometry (PDA) is the works of Anderson et al. (1992) and Ryan et al. (1995). PDA is a point measurement technique that can provide very good spatial resolution. Measurements are typically made a few centimeters below the impingement point at the centerline of the spray.

In the works of Anderson et al. (1992) and Ryan et al. (1995), the arithmetic mean drop diameter was observed to decrease with increasing jet velocity. Drop-size data were recorded at spatial locations 1.6 and 4.1 cm downstream of the impingement point. D_{10} was used to report the mean drop diameters due to the dynamic range difficulty present. Examining the drop-diameter probability density functions in references such as Ryan (1995) shows that the majority of the drops are recorded in the lower end of a dynamic range of approximately 30–1300 μm . As a result, the smallest drops were likely not measured, and the relatively few large drops recorded distorted the mean drop diameters. The authors recognized this and used the D_{10} mean diameter, rather than D_{32} or MMD.

The D_{10} diameters from these studies do not agree well with the established linear stability theories, as outlined by Ryan et al. (1995) and Anderson et al. (2006). However, there exists a possibility that the reason theory and experiments do not agree is because the D_{10} diameter was used instead of D_{32} or MMD, as detailed in a technical note by Ibrahim (2009). Ibrahim (2009) argues that the D_{32} diameters obtained by Kang and Poulidakos (1996) using holography agree well with theory.

In the study by Anderson et al. (1992), the mean drop axial velocities were also presented at spatial locations 1.6 and 4.1 cm downstream of the impingement point at the centerline of the spray. Drop velocities were measured using laser Doppler anemometry (LDA). The drop axial velocity was observed to increase with increasing jet velocity.

There is still a paucity of accurate experimental data for comparison with theoretical models. Developments in PDA since the 1990s have made it possible to measure the small drops that may not have been picked up in previous PDA works by Anderson et al. (1992) and Ryan et al. (1995). In the present study, drop size and drop velocity are quantified

by the PDA technique but without the dynamic range problem in previous works. In other words, the small drops in the spray were also measured in this experimental work. The high-fidelity experimental data in this work provide clarity for comparisons between experiment and theory. In addition, the measured drop axial velocity distributions presented highlight the polydisperse nature of the spray. Different size drops may be traveling at different velocities a few centimeters after breakup due to interactions with the ambient gas environment.

2 Theories of impinging jets

The majority of existing studies in impinging jet atomization have considered the sheet velocity to be equal to the mean jet velocity for theoretical analysis. This is based on the assumption of uniform velocity profile for the jet. Hason and Peck (1964) used the uniform jet velocity profile assumption to calculate the dimensionless sheet thickness parameter K^* , based only on the sheet azimuthal angle ϕ and the half-impingement angle θ . Bremond and Villermaux (2006) and Choo and Kang (2007) have suggested that the uniform jet velocity profile is an assumption that may lead to an incorrect derivation of the sheet characteristics.

The following part closely follows the work of Bremond and Villermaux (2006). The expression for a liquid jet with a Poiseuille parabolic velocity profile can be transformed based on the elliptical cross section at the point of impingement. A schematic of the sheet (as adapted from Bremond and Villermaux 2006) formed by the impinging jets and the jet cross section is provided in Fig. 2. In this figure, b^* is the dimensionless distance from the center of the jet to the separation point, q^* is the dimensionless radial distance from the separation point, and ϕ is the azimuthal angle of the sheet. The terms b^* and q^* are made non-dimensional using the jet radius R_j .

The conservation equations of mass, momentum, and energy are used to derive the sheet velocity and the sheet thickness parameter using the non-uniform jet velocity profile at high jet Weber numbers (neglecting surface tension) and high jet Froude numbers (neglecting gravity). The jet Froude number is defined as:

$$Fr_j = \frac{U_j}{\sqrt{gd_j}}, \tag{7}$$

where g denotes the acceleration due to gravity. The conservation laws under these assumptions are:

$$\text{Mass : } 2 \int_0^{q_j^*} U_j^* \sin \theta q^* d\phi dq^* = U_s^* K^* d\phi, \tag{8}$$

$$\text{Momentum : } \int_0^{2\pi} (U_s^*)^2 K^* \cos \phi d\phi = -4\pi \cos \theta \int_0^{R_j} U_j^2 r dr, \tag{9}$$

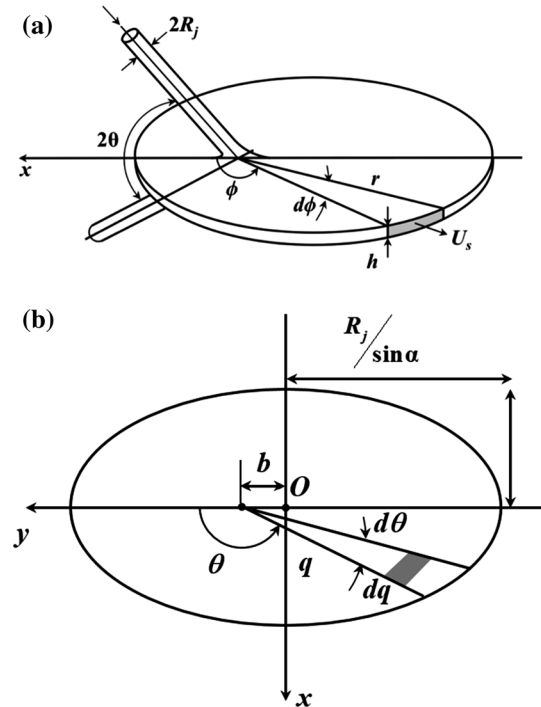


Fig. 2 Schematic of sheet formation (adapted from Bremond and Villermaux 2006): **a** formation of liquid sheet, **b** elliptical cross section of inclined jet. Shaded region indicates the differential volume

$$\text{Energy : } 2 \int_0^{q_j^*} (U_j^*)^3 \sin \theta q^* d\phi dq^* = (U_s^*)^3 K^* d\phi. \tag{10}$$

Here, U_s^* and K^* are the dimensionless sheet velocity and the dimensionless sheet thickness parameters, respectively, under the non-uniform jet velocity profile assumption. The radial location of the jet is symbolized by r . The dimensionless location of the jet interface is denoted by q_j^* and is calculated with the expression:

$$q_j^* = \frac{-b^* \cos \phi \sin^2 \theta + \left(1 - \cos^2 \phi \cos^2 \theta - (b^*)^2 \sin^2 \phi \sin^2 \theta\right)^{0.5}}{1 - \cos^2 \phi \cos^2 \theta} \tag{11}$$

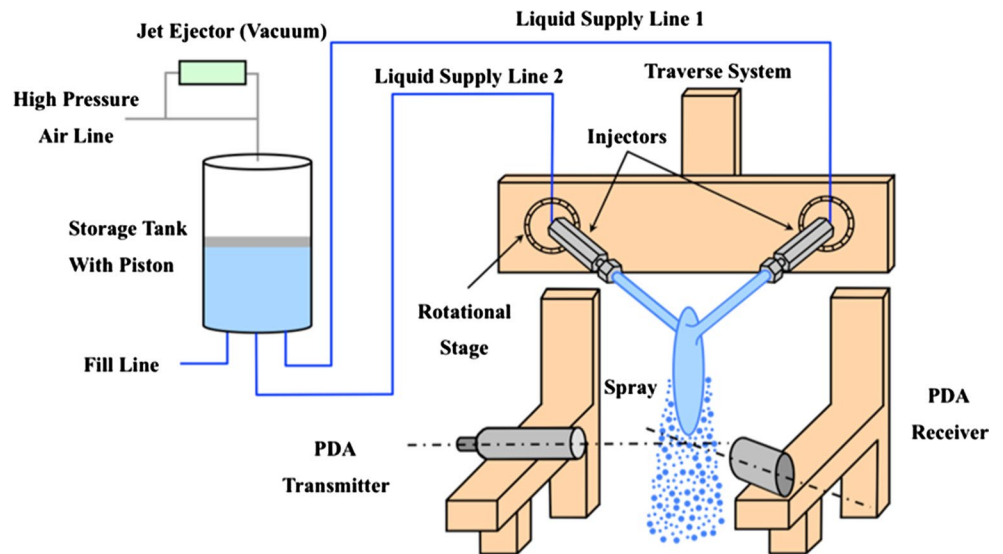
The integrals in Eqs. 8 and 10 have been analytically solved in Bremond and Villermaux (2006) for the parabolic jet velocity profile. The solutions are noted here as:

$$\int_0^{q_j^*} U_j^* q^* dq^* = F(b^*, q^*, \theta, \phi), \tag{12}$$

$$\int_0^{q_j^*} (U_j^*)^3 q^* dq^* = G(b^*, q^*, \theta, \phi). \tag{13}$$

Expressions for the dimensionless sheet velocity and the sheet thickness parameter for the non-uniform jet velocity profile are:

Fig. 3 Experimental apparatus schematic



$$U_s^* = \frac{U_s}{\bar{U}_j} = \left(\frac{G}{F} \right)^{0.5}, \tag{14}$$

$$K^* = \frac{K}{R_j^2} = \frac{xh}{R_j^2} = \frac{(F)^{1.5}}{(G)^{0.5}}. \tag{15}$$

In the above equations, \bar{U}_j is the mean jet velocity, x is the sheet length, and h is the sheet thickness.

Instability analysis has been used in the literature to predict the breakup of the liquid sheet produced by impinging jets. An exhaustive review on the topic can be found in the work of Sirignano and Mehring (2000). Instability analysis yields an expression known as the dispersion relation, which relates the real part of the growth rate of the unstable wave β_r to its wave number k . Dombrowski and Johns (1963) assumed the sinuous wave to be dominant and considered a force balance across the liquid sheet in their analysis. This dispersion relation takes into account the viscous, inertial, surface tension, and the aerodynamic pressure forces. The primary cause of the instability was attributed to aerodynamic interaction of the liquid sheet with the surrounding atmosphere. Neglecting the liquid viscosity, the inviscid dispersion relation based on the force balance is:

$$\frac{\beta_r^2 (h/2)^2}{U_s^2} + \frac{2(k)^2 (h/2)^2}{We_s} - 2sk(h/2) = 0. \tag{16}$$

The sheet Weber number We_s is calculated using the expressions:

$$We_s = \frac{\rho_l U_s^2 h/2}{\gamma}. \tag{17}$$

Two different mechanisms exist in the literature regarding the formation of drops from the breakup of the liquid

sheet. One is a two-stage breakup mechanism proposed by Dombrowski and Johns (1963) and later used by Ryan et al. (1995). In the two-stage breakup mechanism, the sheet first fragments to ligaments and the ligaments then disintegrate to drops. The other is a one-step direct breakup mechanism proposed by Ibrahim and Przekwas (1991), where drops are directly formed from the liquid sheet.

Of particular importance for analytical drop-size predictions are the sheet thickness parameter K and the sheet velocity U_s . In this work, the sheet characteristics derived by Bremond and Villermaux (2006) will be extended to predict drop sizes. Furthermore, their sheet formation analysis will be emulated for the case of the 1/7th power law turbulent jet velocity profile, and drop sizes will also be predicted based on this jet velocity profile.

3 Experimental facilities

The unique experimental apparatus used to create atomization in this study was essentially identical to the facility used by Mallory and Sojka (2014) and Rodrigues and Sojka (2014). Figure 3 provides a schematic of the facility. Drop-size measurements were made at dimensionless numbers range of $6820 < We_j < 21,900$; $18,500 < Re_j < 33,100$; and $328 < Fr_j < 588$. Rotational stages were used to specify the impingement angle 2θ . Translation stages were used to specify the free jet length-to-orifice diameter ratio x/d . Designated tip elements were used to specify the internal length-to-orifice diameter ratio L/d and the orifice diameter d_0 . The operating pressure was varied to change the mean jet velocity \bar{U}_j . The geometric parameters were $d_0 = 0.686$ mm, $2\theta = 100^\circ$, $x/d = 60$, $L/d = 20$. Deionized water was used as the test liquid, and the literature values are used for liquid density ($\rho_l = 1000$ kg/m³) and

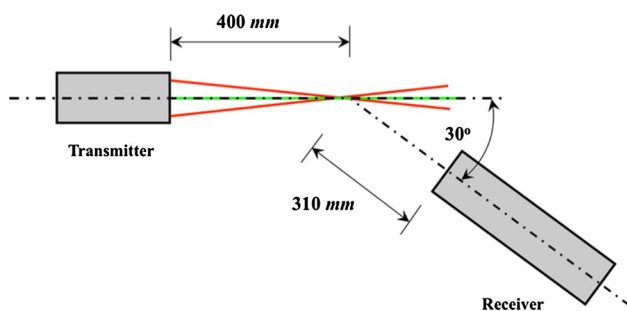


Fig. 4 PDA setup schematic

liquid viscosity ($\mu_l = 0.001$ Pa s). The ambient gas was air at atmospheric temperature and pressure; literature values were used for gas density ($\rho_g = 1.2$ kg/m³) and gas viscosity ($\mu_g = 1.85E-05$ Pa s). The liquid/gas surface tension was taken to be the literature value of water/air at atmospheric conditions ($\gamma = 0.0728$ N/m). The mean jet velocity was measured using a stopwatch for flow rate test durations of 30 s. Flow rate measurements were repeated three times to ensure statistically significant mean jet velocity measurements. The flow exiting the orifice is believed to be turbulent due to the high Reynolds numbers. A discharge coefficient of 0.70 ± 0.02 was measured for the orifices. Cavitation was not visibly observed for the test conditions used in this work, despite the high jet velocities. This can be attributed to the fairly high L/d ratio and the rather small orifice diameter.

A PDA system was used to obtain measurements of drop size and drop velocity. Phase Doppler anemometry (PDA) measures the drop diameter by measuring the phase difference between Doppler signals from two different detectors. The drop velocity can also be measured by the PDA system by measuring the frequency of the Doppler bursts, which are obtained by converting the optical signals from the detectors. These Doppler bursts have a frequency that is linearly proportional to the drop velocity. More details about the theory behind PDA may be found in Albrecht et al. (2003). The PDA receiver with a 310-mm focal length lens was oriented 30° from the laser beams produced by the PDA transmitter. The PDA transmitter emits a pair of

Helium–Neon and Nd:YAG laser beams and was used with a 400-mm focal length lens. Figure 4 provides a schematic of the setup for the PDA optical diagnostics.

The PDA was configured with particular hardware and software settings to yield high validation and data rates. All measurements were taken at the centerline of the spray at 5 cm below the point of impingement. The injector pair was mounted on traverse stages that enable movement in all three spatial dimensions for alignment. 50,000 data points were collected for each test. A curtain of air was placed in front of the PDA receiver using an air-knife to prevent drops from some test conditions from landing on the lens. Measurements were taken with and without the air curtain at a baseline condition for comparison to ensure that the air does not have an effect on the measurements.

The PDA optical configuration enables a drop-size measurement range between approximately 2.3–116.2 μm by using the selected aperture plate (Mask B). This was chosen as the optimal measurement range over two other options of 1.4–71.6 μm (Mask A) and 5.5–276.8 μm (Mask C). A truncation analysis showed that Mask C did not detect the small drops that were detected by the other two masks. Mask B was observed to not only detect the small drops that were detected by Mask A, but also detect the larger drops that were not detected by Mask A. Further details on the aperture plate selection can be found in Rodrigues (2014). In direct contrast, recall that the drop-size measurement range used by Anderson et al. (1992) and Ryan et al. (1995) was about 30–1300 μm . The smallest drops were certainly not detected in the previous works.

The experimental setup for imaging the impinging jets is shown in Fig. 5. The back illumination was provided by a double-pulsed Nd:YAG laser beam. The pulse width was 6 ns, which is short enough to freeze the motion of the liquid. The laser beam was first expanded and then projected to a diffuser, thus significantly reducing the coherence of the laser beam. Accordingly, no interference patterns were observed in the recorded images. In addition, the effect of the speckle noise on image quality was unnoticeable due to the relatively small speckle size. A CCD camera was focused at the plane of the two impinging jets, which was back-illuminated by the light produced by the diffuser.

Fig. 5 Schematic for imaging system

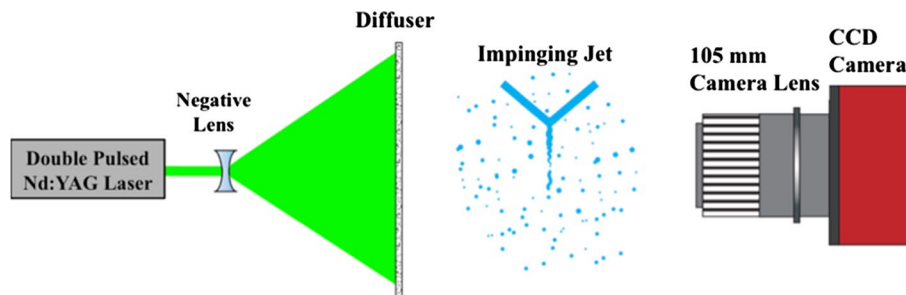


Table 1 Experimental uncertainty for presented experimental data

Quantity	Uncertainty (%)
We_j	4.5
D_{10}	5.9
D_{32}	1.3
MMD	0.9
U_{z-mean}	2.9

Table 1 provides the percent uncertainty for the experimental work. The percent uncertainty for the operating conditions was calculated using the method delineated in Kline and McClintock (1953). Mean drop diameters (D_{10} , D_{32} , MMD) and mean axial drop velocity (U_{z-mean}) uncertainties were investigated by taking five repeated measurements at a baseline operating condition. The coefficient of variation, the ratio of one standard deviation to the mean, was used as the uncertainty for the PDA measurements. Further details on calculating the uncertainty can be found in Rodrigues (2014).

4 Results and discussion

Figure 6 presents a selection of number, surface area, and volume probability density functions (pdf) along with the corresponding spray patterns for increasing jet Weber numbers. It was observed that the sheet breaks up a short distance from the point of impingement. An increase in the denseness of the spray with increasing jet Weber numbers was also observed, which was consistent with the greater data rate in the PDA measurements at higher We_j . The number pdf was not observed to vary significantly with increasing jet Weber numbers. This is likely due to the high quality of atomization in the impact wave regime. However, variations were observed in the surface area and volume pdfs, which indicates that a smaller portion of larger drops is present at higher jet Weber numbers.

Experimental values of D_{10} , D_{32} , and MMD are presented as a function of the jet Weber number in Fig. 7. The D_{10} drop diameter was not significantly affected by an increase in We_j , due to the large number of small drops spanning the range of jet Weber number. However, the decrease in the D_{32} mean diameter indicates that the fineness of the spray was improved by the enhancement of the inertial force. MMD was also observed to decrease with increasing We_j . In this work, MMD is used for comparison with analytical diameter predictions because the instability model is based on a momentum balance and therefore must have a mass/volume foundation to it.

In Bremond and Villiermaux (2006), the momentum equation (Eq. 9) was numerically solved in order to

determine the value for b^* , the dimensionless distance from the center of the jet to the separation point. It was determined that $b^* = 0.68/\tan\theta$ for the parabolic jet velocity profile. For a 1/7th power law turbulent jet velocity profile, the dimensionless velocity profile is given by:

$$U_{j,t}^* = \frac{U_{j,t}}{U_j} = 1.22 \left(1 - \frac{r}{R_j}\right)^{\frac{1}{7}} \tag{18}$$

In the above expression, $U_{j,t}$ is the dimensional turbulent jet velocity and r is the radial location of the jet. The maximum velocity of 1.22 times the mean jet velocity occurs at $r = 0$ (jet centerline), and the minimum velocity of 0 occurs at $r = R_j$ (jet edge). Equation 9 was numerically solved for the turbulent jet velocity profile for a half-impingement angle of 50° to yield $b^* = 0.755$. Using this value for the dimensionless distance from the center of the jet to the separation point, Eqs. 11–15 were solved for the turbulent jet velocity profile. Table 2 presents the values for b^* , ratio of sheet velocity to mean jet velocity α , and dimensionless sheet thickness parameter K^* for the uniform, parabolic, and turbulent jet velocity profiles at the corresponding experimental conditions (impingement angle $2\theta = 100^\circ$ and sheet azimuthal angle $\phi = 0^\circ$).

Squire (1953) used the long-wave approximation ($kh/2 \ll 1$) to solve the dispersion relation for the maximum growth rate $\beta_{r,max}$ and its corresponding wave number k_{max} . These are expressed as:

$$\beta_{r,max} = \frac{\rho_g U_s^2}{\sqrt{2\rho_l \gamma h}}, \tag{19}$$

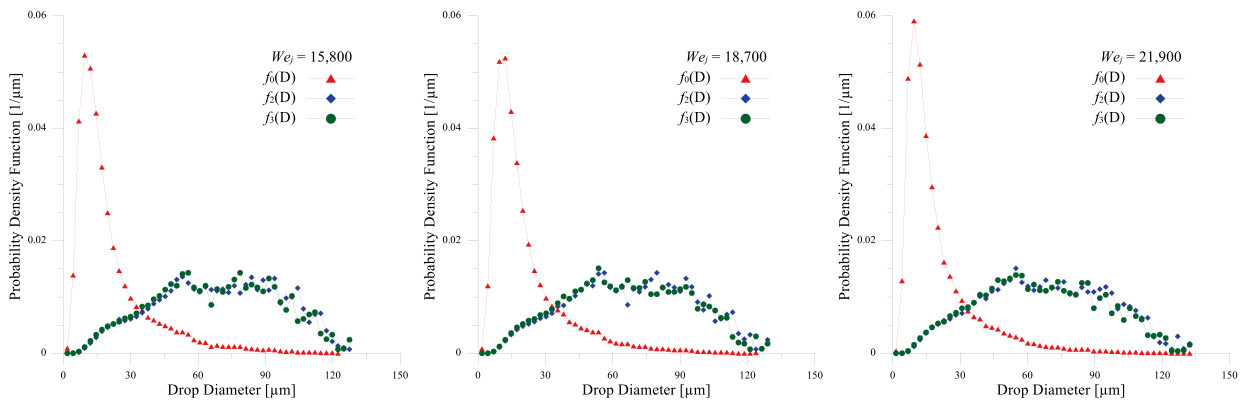
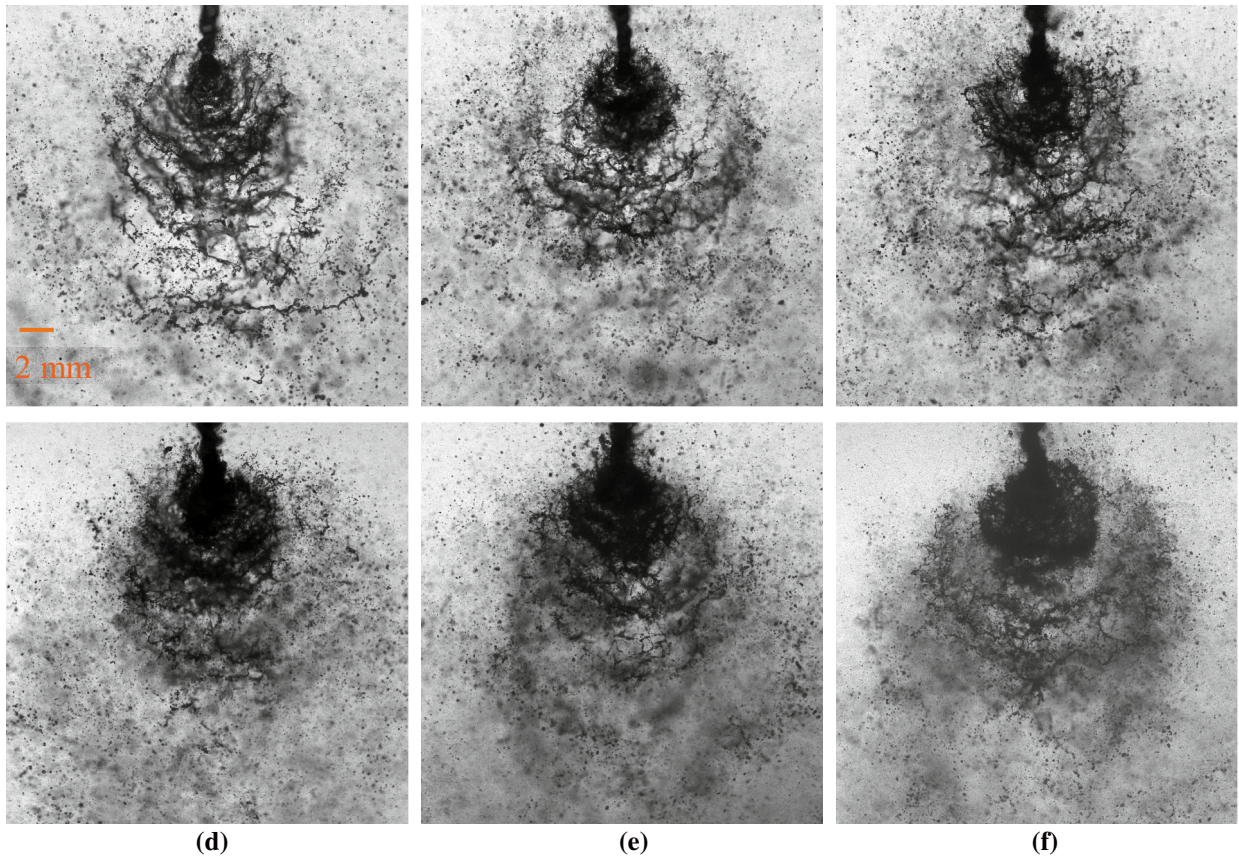
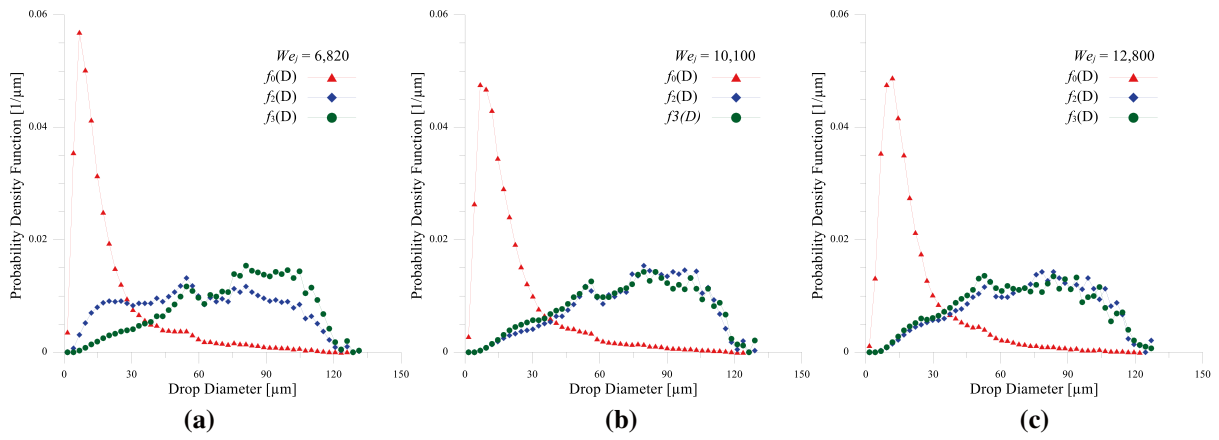
$$k_{max} = \frac{\rho_g U_s^2}{2\gamma}. \tag{20}$$

In the one-step breakup mechanism by Ibrahim and Przekwas (1991), it is assumed that sheet breakup is due to the growth of waves at the maximum amplification rate. The resulting drop size is determined as half of the wavelength of the fastest growing waves λ_{max} . Since $k_{max} = 2\pi/\lambda_{max}$:

$$d_D = \frac{\pi}{k_{max}}. \tag{21}$$

Equations 20 and 21 can be combined and the dimensionless drop diameter can be expressed in terms of the jet Weber number We_j , ratio of sheet velocity to mean jet velocity α , and ratio of ambient gas density to liquid density s . The resulting analytical expression for the drop diameter is dependent on the assumed jet velocity profile:

$$\frac{d_D}{d_0} = \frac{2\pi}{\alpha^2 s We_j}. \tag{22}$$



◀ **Fig. 6** Number, area, and volume pdfs versus drop diameters with corresponding spray patterns for: **a** $We_j = 6280$, **b** $We_j = 10,100$, **c** $We_j = 12,800$, **d** $We_j = 15,800$, **e** $We_j = 18,700$, **f** $We_j = 21,900$

For the case of the uniform jet velocity profile, $\alpha = 1$, Eq. 22 is reduced to the expression proposed by Ibrahim and Przekwas (1991):

$$\frac{d_D}{d_0} = \frac{2\pi}{sWe_j} \tag{23}$$

One obvious disadvantage of the one-step breakup mechanism is the lack of dependency on the sheet azimuthal angle and half-impingement angle.

A condition for breakup needs to be first established for the two-step breakup mechanism. Dombrowski and Johns (1963) based the criterion for sheet breakup on the following empirical relation:

$$\int_0^{x_b} \frac{\beta_{r,max}}{U_s} dx = 12, \tag{24}$$

where x_b is the sheet breakup length. The choice of the constant 12 is based on experimental observations by Weber (1931). This expression is for an attenuating sheet, and

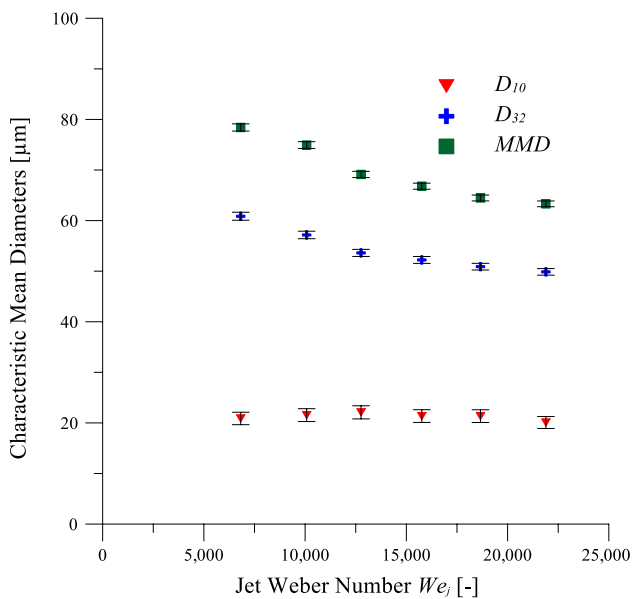


Fig. 7 Experimentally measured D_{10} , D_{32} , and MMD versus jet Weber number

Table 2 Calculated dimensionless parameters for three jet velocity profiles at $2\theta = 100^\circ$, $\phi = 0^\circ$

Jet velocity profile	b^*	α	K^*
Parabolic	0.571	1.61	1.34
Turbulent	0.755	1.08	2.07
Uniform	0.839	1.00	3.52

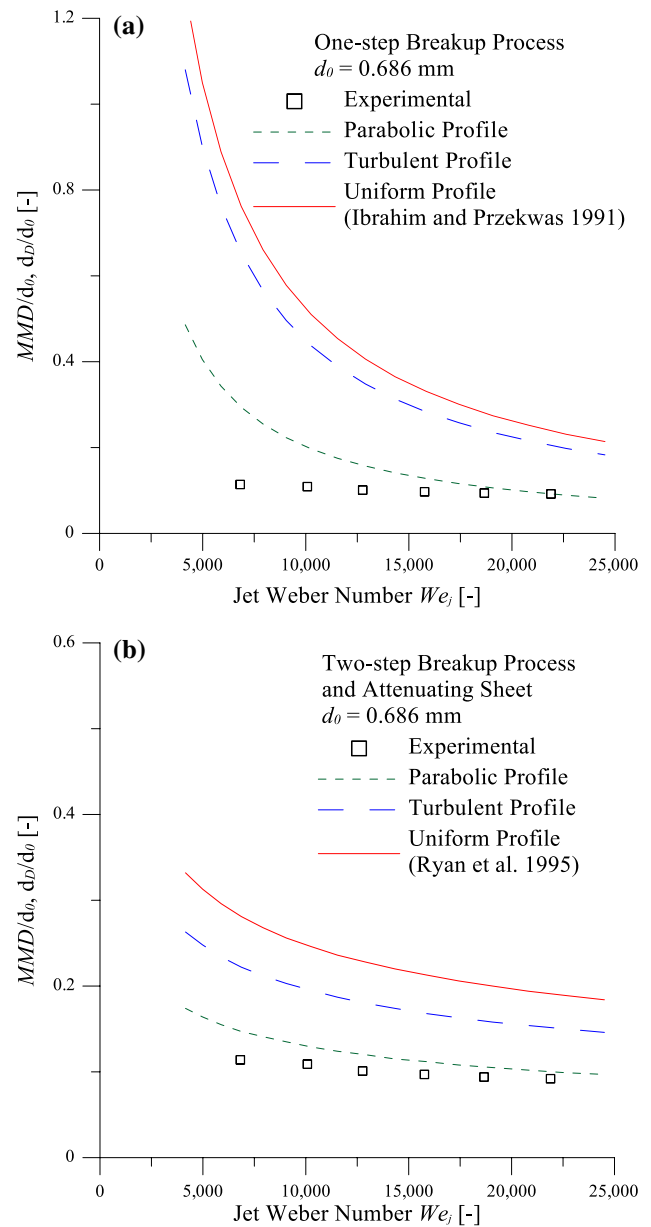


Fig. 8 Dimensionless mass median diameter and predicted drop diameters versus jet Weber number for: **a** one-step breakup mechanism, **b** two-step breakup mechanism with attenuating sheet

therefore, the growth rate must be integrated to predict the breakup length. The sheet breakup length is used with the sheet thickness parameter K to calculate the sheet thickness at breakup h_b :

$$K = x_b/h_b. \tag{25}$$

Dombrowski and Johns (1963) then calculated the ligament diameter d_L using the expression:

$$d_L = \sqrt{\frac{4h_b}{k_{max}}}. \tag{26}$$

In practice, curved ligaments break off from the sheet, as observed in the images of Ryan et al. (1995) among others. However, the curvature of the ligaments is large compared to their diameter. As argued by Dombrowski and Johns (1963), this permits the use of the Plateau–Rayleigh analysis to calculate the drop diameter d_D :

$$d_D = 1.88d_L. \tag{27}$$

Combining the expressions in Eqs. 19, 20, 24–27, the dimensionless drop diameter can be expressed in terms of the jet Weber number We_j , ratio of sheet velocity to mean jet velocity α , dimensionless sheet thickness parameter K^* , and ratio of ambient gas density to liquid density s :

$$\frac{d_D}{d_0} = \frac{1.14(K^*)^{1/3}}{\alpha^{2/3}s^{1/6}We_j^{1/3}}. \tag{28}$$

For the case of the uniform jet velocity profile, $\alpha = 1$, Eq. 28 is reduced to the expression proposed by Ryan et al. (1995):

$$\frac{d_D}{d_0} = \left[\frac{2.62}{12^{1/3}} \right] s^{-1/6} [We_j f(\theta)]^{-1/3}, f(\theta) = \frac{(1 - \cos \phi \cos \theta)^2}{\sin^3 \theta}. \tag{29}$$

Note that for the case of the uniform jet velocity profile, $K^* = 1/f(\theta)$.

In this experimental work, the jets did not have a parabolic profile inside the orifice and instead likely had a turbulent profile due to the large jet Reynolds numbers. However, as argued by Bremond and Villermaux (2006), considering the parabolic profile is a worthwhile investigation of another limit to complement the investigated models of prior researchers who studied the uniform velocity profile limit. Diameter predictions from parabolic, turbulent, and uniform velocity profiles are presented in this work.

Figure 8a presents a comparison of the experimental MMD and predicted diameters using the one-step breakup process for the parabolic, turbulent, and uniform velocity profiles. It can be clearly observed that predictions from the uniform profile used by Ibrahim and Przekwas (1991) drastically overpredict the experimental MMD. This can be attributed to the assumption of uniform velocity profile, which leads to the sheet velocity being equal to the jet velocity. Diameter predictions closer to the experimental data were observed for the turbulent and parabolic jet velocity profiles. However, note that the trends from all three models that use this one-step breakup process did not agree with the trends of the experimental MMD. This is because Eq. 22 does not satisfactorily capture the nonlinearity in the atomization process.

A comparison of the experimental MMD to the predicted diameters given by the two-step breakup mechanism with the attenuating sheet for parabolic, turbulent, and

uniform jet velocity profiles is presented in Fig. 8b. Once again it can be clearly observed that predictions from the uniform profile used by Ryan et al. (1995) significantly overpredict the experimental MMD. Diameter predictions from the turbulent jet velocity profile offer a closer comparison to the experimental data, and predictions from the parabolic jet velocity provide almost an exact match.

An empirical correlation with an $R^2 = 0.97$ for drop diameter based on the experimental MMD is:

$$\frac{d_D}{d_0} = \frac{0.325}{s^{1/6}We_j^{0.201}}. \tag{30}$$

It should be noted that the only density ratio tested for this experimental work was air to water, both at atmospheric conditions. Therefore, the Ryan et al. (1995) exponent of $-1/6$ for the density ratio is assumed here. The jet Weber number range tested was from 6820 to 21,900. The exponent for We_j presented here (0.201) is lower than those of the one-step breakup mechanism (1) and two-step breakup mechanism (1/3). This indicates a weaker dependency on We_j according to the experimental data. Therefore, although trends from the two-step breakup mechanism agree better than trends from the one-step breakup mechanism, further work is needed to incorporate more of the nonlinearity.

Higher mean drop velocities were observed with an increase in the jet Weber number, due to the increase in the inertial force. Experimental values of the drop axial velocity are compared with a model based on drop ballistics theory. Equation 31 provides the standard governing ordinary differential equation used to calculate the drop velocity U_d based on the axial position x . The equation balances the inertial force with the gravitational force and drag force:

$$\frac{dU_d}{dx} = \frac{g}{U_d} - \frac{3C_{drag}}{4d_D} sU_d. \tag{31}$$

In the above expression, C_{drag} is the drag coefficient and is calculated using the criteria:

$$C_{drag} = \begin{cases} 24/Re_D, & Re_D < 2 \\ 18.5/Re_D^{0.6}, & 2 < Re_D < 1000 \\ 0.44, & 1000 < Re_D. \end{cases} \tag{32}$$

The drop Reynolds number is calculated using the expression:

$$Re_D = \frac{\rho_g U_D d_D}{\mu_g}. \tag{33}$$

The drop diameter used to calculate the Reynolds number of the drop Re_D was the experimentally determined D_{32} . D_{32} was used as the mean diameter because the surface area and volume of the drop are the basis for the drop ballistics model. Literature values for air at atmospheric conditions were used for the gas density ρ_g and gas viscosity μ_g . The

initial velocity of the drop U_d was assumed to be the velocity of the sheet at $\phi = 0^\circ$. The sheet velocity is dependent on the jet velocity profile assumed (parabolic, turbulent, or uniform). The drop Weber number We_D is calculated using the expression:

$$We_D = \frac{\rho_g U_D d_D}{\gamma} \tag{34}$$

The experimentally determined D_{32} was also used as the drop diameter to calculate We_D . The calculated drop Weber numbers ($0.19 < We_D < 0.51$) were well below the established regimes for secondary atomization (Guildenbecher et al. 2009). Therefore, surface tension effects connected with the drop deformation were neglected in this drop ballistics model.

The initial location of the drop was assumed to be the sheet breakup length. This was calculated using a phenomenological relation (Anderson et al. 2006):

$$\frac{x_b}{d_0} = 13.56 \left(We_j s^2 \right)^{-0.102} \tag{35}$$

Experimental diameter data and a phenomenological relation for breakup length were used instead of predictions based on instability analysis in order to ensure that deficiencies in the instability theory were not introduced into the drop ballistics model.

Comparisons between theoretical predictions based on the three jet velocity profiles and experimental data are presented in Fig. 9. It should be noted that the experimental uncertainty is within the symbol, and the vertical bars shown are the root mean square (RMS) of velocity. The predictions with the turbulent jet velocity profile agree best with the experimental data. Predictions with the parabolic jet velocity profile overpredict the drop velocities, and predictions with the uniform velocity profile slightly underpredict the drop velocities. These observations are directly related to the initial velocity of the drop, which in turn ultimately depends on the ratio of sheet velocity to mean jet velocity α . Velocity predictions based on the turbulent $\alpha = 1.08$ agree best with the experimental drop velocities, since the turbulent jet velocity profile most closely corresponds with the experiment condition.

Due to the large root mean square values, a more detailed look at the drop velocities is required. The pdfs of drop velocities at different jet Weber numbers are shown in Fig. 10, where relative velocity obtained by subtraction of the mean drop velocity is presented. At higher We_j , it was observed that there is a shorter/flatter peak for the drop velocity with the greatest probability density. The distribution was also observed to become increasingly wider. This indicated that at the higher jet Weber numbers, the drop velocities in the spray become increasingly polydispersed.

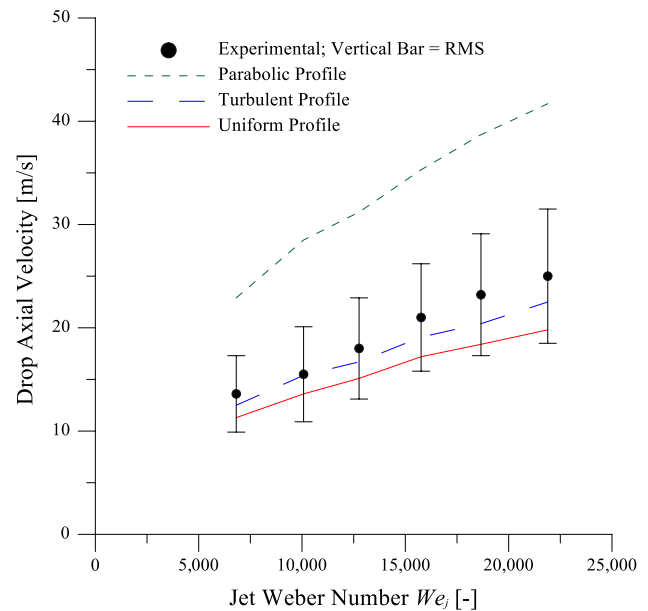


Fig. 9 Measured and predicted drop axial velocity versus jet Weber number

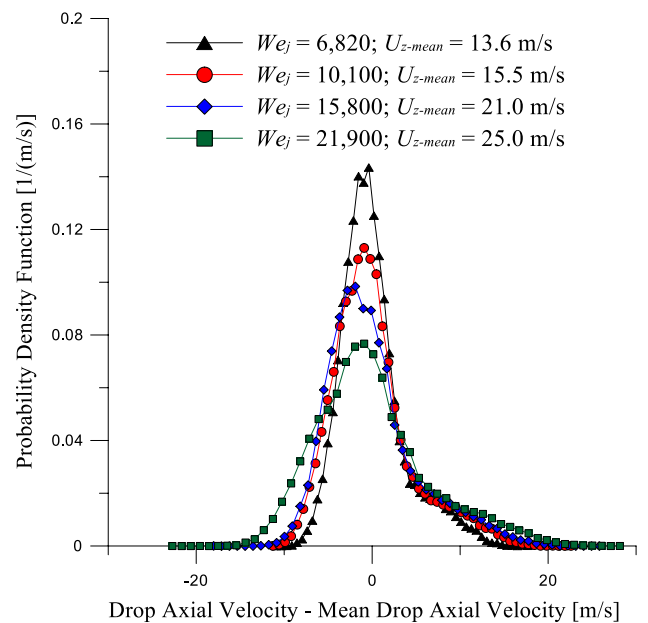


Fig. 10 Measured axial velocity pdf versus drop axial velocity minus mean drop axial velocity

5 Conclusions

In the experimental portion of this work, measurements were presented for the means and distribution of drop diameter and drop velocity in the impact wave regime. A modern PDA system that has the capacity to measure the smallest drops in the spray was used in order to correct the

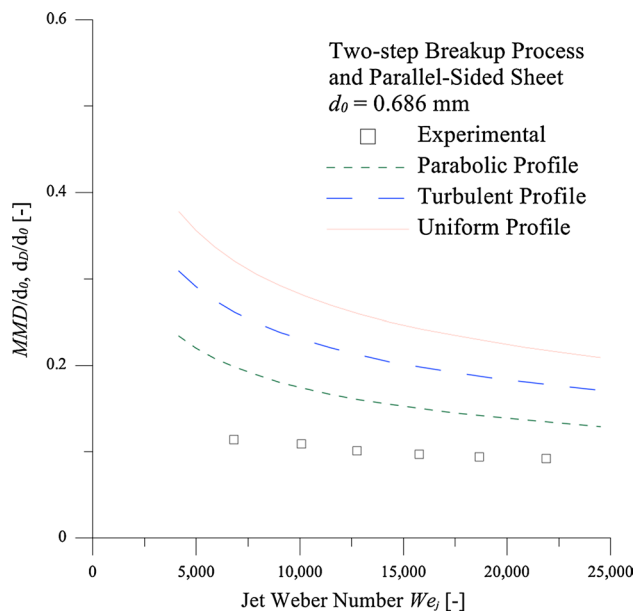


Fig. 11 Dimensionless mass median diameter and predicted drop diameters versus jet Weber number for two-step breakup mechanism with parallel-sided sheet

dynamic range problem from the previous studies. Number, surface area, and volume pdfs provided an indication of the variety of drop sizes in the spray. The D_{32} and MMD drop diameters were observed to decrease with increasing We_j , which was due to a decrease in the number of larger drops at higher jet Weber numbers. The mean drop velocity was observed to increase with increasing We_j . This was due to the increased inertial force at higher jet Weber numbers. Probability density functions of drop velocity were presented, and a wider distribution for drop velocities was observed at higher We_j . This indicates an enhancement of the polydisperse nature of the spray as the inertial force was increased.

The importance of the assumed jet velocity profile on analytical drop diameter predictions was illustrated in this work. Analytical drop diameter models in literature, which assume a uniform jet velocity profile, showed poor agreement with experimental MMD for both one-step and two-step breakup mechanism. Analytical expressions that depend on parameters based on the assumed jet velocity profile were presented for both the one-step and two-step breakup mechanism. Predictions based on the parabolic and turbulent jet velocity profiles using the two-step breakup mechanism showed close agreement with the experimental data. For all jet velocity profiles, predictions using the one-step breakup mechanism showed poor agreement with the experimental data. Velocity predictions from the drop ballistics model using the turbulent jet velocity profile agreed best with the experimentally measured mean drop velocities.

Acknowledgments The research presented in this paper was made possible with the financial support of the U.S. Army Research Office under the Multi-University Research Initiative Grant Number W911NF-08-1-0171. N. S. Rodrigues thanks Prof. Jennifer Mallory for helpful feedback, Dr. Ariel Muliadi for assistance with PDA configuration, and Prof. William Anderson for fruitful discussions.

Appendix

For the assumption of a parallel-sided sheet, instead of an attenuating sheet, the sheet thickness is constant. Therefore, as outlined in Senecal et al. (1999), the following expression can be used as a condition for breakup:

$$\frac{x_b \beta_{r,\max}}{U_s} = 12. \quad (36)$$

In keeping with the long-wave approximation ($kh/2 \ll 1$), an analytical expression can also be derived for drop diameter. This expression depends on the jet Weber number We_j , ratio of sheet velocity to mean jet velocity α , dimensionless sheet thickness parameter K^* , and ratio of ambient gas density to liquid density s :

$$\frac{d_D}{d_0} = \frac{1.30(K^*)^{1/3}}{\alpha^{2/3}s^{1/6}We_j^{1/3}}. \quad (37)$$

Figure 11 presents a comparison of the experimental MMD to the predicted diameters given by the two-step breakup mechanism with the parallel-sided sheet for parabolic, turbulent, and uniform jet velocity profiles. The parallel-sided sheet assumption is useful for predictions for viscous Newtonian and non-Newtonian liquids, where the inviscid assumption cannot be justified.

References

- Albrecht HE, Borys M, Damaschke N, Tropea C (2003) Laser doppler and phase doppler measurement techniques. Springer, Berlin
- Anderson WE, Ryan HM, Pal S, Santoro RJ (1992) Fundamental studies of impinging liquid jets. AIAA. Paper No. 92-0458
- Anderson WE, Ryan HM, Santoro RJ (1995) Impinging jet injector atomization. In: Yang V, Anderson WE (eds) Liquid rocket engine combustion instability. Progress in Astronautics and Aeronautics, Washington, DC, pp 215–246
- Anderson WE, Ryan HM, Santoro RJ (2006) Impact wave-based model of impinging jet atomization. Atomization Sprays 16:791–805
- Bremond N, Villermaux E (2006) Atomization by jet impact. J Fluid Mech 549:273–306
- Choo YJ, Kang BS (2007) The effect of jet velocity profile on the characteristics of thickness and velocity of the liquid sheet formed by two impinging jets. Phys Fluids A 19:11
- Dombrowski ND, Hooper PC (1963) A study of the sprays formed by impinging jets in laminar and turbulent flow. J Fluid Mech 18:392–400
- Dombrowski ND, Johns WR (1963) The aerodynamic instability and disintegration of viscous liquid sheets. Chem Eng Sci 18:203–214

- Gill GS, Nurick WH (1976) Liquid rocket engine injectors. NASA SP-8089
- Guildenbecher DR, López-Rivera C, Sojka PE (2009) Secondary atomization. *Exp Fluids* 46:371–402
- Hasson D, Peck RE (1964) Thickness distribution in a sheet formed by impinging jets. *AIChE J* 10:752–754
- Heidmann MF, Priem RJ, Humphrey JC (1957) A study of sprays formed by two impinging jets. NACA TN D-301
- Heister SD (2011) Pintle Injectors. In: Ashgriz N (ed) *Handbook of atomization and sprays*. Springer, New York, pp 647–655
- Humble RW, Henry GN, Larson WJ (1995) *Space propulsion analysis and design*. McGraw-Hill, New York
- Ibrahim EA (2009) Comment on “Atomization characteristics of impinging liquid jets”. *J Propuls Power* 25:1361–1362
- Ibrahim EA, Przekwas AJ (1991) Impinging jets atomization. *Phys Fluids A* 3:2981–2987
- Kang BS, Poulidakos D (1996) Holography experiments in a dense high-speed impinging jet spray. *J Propuls Power* 12:341–348
- Kline SJ, McClintock FA (1953) Describing uncertainties in single-sample experiments. *Mech Eng* 75:3–8
- Lefebvre AH (1989) *Atomization and sprays*. Hemisphere, New York
- Mallory JA, Sojka PE (2014) On the primary atomization of non-Newtonian impinging jets: volume I experimental investigation. *Atomization Sprays* 24:431–465
- Rodrigues NS (2014) Impinging jet spray formation using non-Newtonian liquids. MS thesis, Purdue University
- Rodrigues NS, Sojka PE (2014) A parametric investigation of gelled propellant spray characteristics utilizing impinging jet geometry. AIAA. Paper No. 2014-1184
- Ryan HM (1995) Fundamental study of impinging jet atomization. PhD dissertation, The Pennsylvania State University
- Ryan HM, Anderson WE, Pal S, Santoro RJ (1995) Atomization characteristics of impinging liquid jets. *J Propuls Power* 11:135–145
- Senecal PK, Schmidt DP, Nouar I, Rutland CJ, Reitz RD, Corradini ML (1999) Modeling high-speed viscous liquid sheet atomization. *Intl J Multiph Flow* 25:1073–1097
- Sirignano WA, Mehring C (2000) Review of theory of distortion and disintegration of liquid streams. *Prog Energy Comb Sci* 26:609–655
- Squire HB (1953) Investigation of the instability of a moving liquid film. *Brit J Applied Phys* 4:167–169
- Vingert L, Gicquel P, Lourme D, Menoret L (1995) Coaxial injector atomization. In: Yang V, Anderson WE (eds) *Liquid rocket engine combustion instability*. Progress in Astronautics and Aeronautics, Washington, DC, pp 145–190
- Von Kampen J, Madlener K, Ciezki HK (2006) Characteristic flow and spray properties of gelled fuels with regard to the impinging jet injector. AIAA. Paper No. 2006-4573
- Weber C (1931) Disintegration of liquid jets. *Zeitschrift für Angewandte Mathematik und Mechanik* 11:136–159